5
Baryonic matter in light of astrophysical observations

5.1 Introduction

The understanding of dense matter above n_0 can be reasonably improved using recent compact star observations as the constraints on lower limit of maximum mass, observed range of mass-radius of certain compact stars and most importantly the compactness from observed tidal deformability. The soft EoS of highly dense matter can be ruled out from the observations of massive stars viz. PSR J1614 − 2230 ($M = 1.908 \pm 0.016\ M_\odot$) [Demorest et al., 2010; Arzoumanian et al., 2018], PSR J0348 + 0432 ($2.01 \pm 0.04\ M_\odot$) [Antoniadis et al., 2013], millisecond pulsar J0740 + 6620 ($2.14^{+0.20}_{-0.18}\ M_\odot$ with 95% credibility [Cromartie et al., 2020], $2.08^{+0.07}_{-0.07}\ M_\odot$ with 68.3% credibility [Fonseca et al., 2021]) and PSR J1810+1744 ($2.13\pm0.04\ M_\odot$ with 68% credibility) [Romani et al., 2021].

Gravitational-wave observations also can constrain well the models of highly dense matter as already stated in chapter-1. For low-spin prior systems from GW170817 event, it is estimated that the combined dimensionless tidal deformability ($\tilde{\Lambda}$) parameter value has an upper and lower bounds of 900 (TaylorF2 model) [Abbott et al., 2017c] and 400 (AT2017gfo event) [Radice et al., 2018] respectively. Reanalysis of the GW170817 data by LVC has set new limits as $110 \leq \tilde{\Lambda} \leq 720$ (PhenomPNRT model) [Abbott et al., 2019]. Another estimation of $\tilde{\Lambda}$ based on the viability of chiral effective field theory results provides the limit to be in the range $80 \leq \tilde{\Lambda} \leq 570$ [Tews et al., 2018]. In addition, an improved analysis of GW170817 event data implementing identical EoS for both the compact stars producing rational waveforms provides a limit on the dimensionless tidal deformability (Λ) for a $1.4M_\odot$ NS to be in the range $70 \leq \Lambda_{1.4} \leq 580$ with 90% credibility [Abbott et al., 2019]. Raithel et al. [2018] reported that the $\tilde{\Lambda} \leq 800$ constraint implies the radius of primary compact object to be < 13 km.

Another gravitational-wave observation (GW190814) by the LIGO Livingston detector (LVC) inferred to be from a coalescence of a black-hole (BH) and lighter compact object appendage with mass of the latter to be $2.59^{+0.08}_{-0.09}\ M_\odot$ [Abbott et al., 2020b] which falls in the 'mass-gap'. The nature of lighter companion is still not resolved [Most et al., 2020; Tews et al., 2021; Sedrakian et al., 2020; Jie Li et al., 2020; Dexheimer et al., 2021; Bombaci et al., 2021; Fattoyev et al., 2020].

Along with this, we get good information about mass-radius relation of compact stars from NICER observations. This space mission recently provided adequate information to estimate the mass-radius of PSR J0030 + 0451 to be in the range of $1.44^{+0.15}_{-0.14}\ M_\odot$, $13.02^{+1.24}_{-1.06}$ km

[Miller et al., 2019] and $1.34^{+0.15}_{-0.16}$ $M_\odot$, $12.71^{+1.14}_{-1.19}$ km (with 68.3% credibility) [Riley et al., 2019] respectively. Latest estimate of mass-radius of PSR J0740 + 6620 by NICER is in the range of $2.072^{+0.067}_{-0.066}$ $M_\odot$, $12.39^{+1.30}_{-0.98}$ km [Riley et al., 2021] and 2.08 ± 0.07 $M_\odot$, $13.71^{+2.62}_{-1.50}$ km (with 68% credibility) [Miller et al., 2021] respectively. Several works [Zhang and Li, 2021; Biswas, 2021; Pang et al., 2021; Raaijmakers et al., 2021; Somasundaram and Margueron, 2021; Li et al., 2021a] have been performed based on different analyses on astrophysical observations inclusive of the latest NICER measurements to extract new information regarding dense matter EoS.

An estimation for tidal deformability from NICER observations of PSR J0030 + 0451 jointly with GW170817 event provides $240 \leq \Lambda_{1.4} \leq 730$ with radius range as $R_{1.4} = 12.1^{+1.2}_{-0.8}$ km [Jiang et al., 2020]. Another recent analysis of the same PSR J0030 + 0451 data (NICER) reveals $R_{1.4} = 12.32^{+1.09}_{-1.47}$ km [Landry et al., 2020]. The radius constraint on the $1.4M_\odot$ NSs from the GW170817 event has been derived to be in the range $10.5 \leq R_{1.4}/\text{km} \leq 13.4$ [Abbott et al., 2019] while Malik et al. [2018] provide the radius limit to be $11.82 \leq R_{1.4}/\text{km} \leq 13.72$. Considering similar low-spin prior systems for the GW190425 event, an upper bound of 600 (PhenomPv2NRT model) has been placed on $\tilde{\Lambda}$ and the radius upper limit is derived as $R < 15$ km [Abbott et al., 2020a].

From the analysis of GW170817 event data, bounds on matter pressure ranges are derived at $2n_0$ and $6n_0$ to be $3.5^{+2.7}_{-1.7} \times 10^{34}$ dyn-cm^{-2} and $9.0^{+7.9}_{-2.6} \times 10^{35}$ dyn-cm^{-2} respectively [Abbott et al., 2018]. Recent results obtained from GW170817 event by Bayesian analysis suggest matter pressure at $2n_0$ to be $\sim 3.81^{+1.18}_{-2.32} \times 10^{34}$ dyn/cm^2 and $133 \leq \Lambda_{1.4} \leq 686$ [Li et al., 2021b]. The analysis of GW190425 event data reveals core matter density of the primary component involved to be in the range $3 \leq n/n_0 \leq 6$ and matter pressure to be in $10^{35} \leq P(3 - 6\ n_0) \leq 8 \times 10^{35}$ dyn/cm^2 range [Abbott et al., 2020a].

In this work, we employ the available constraints obtained so far from compact object observations to narrow down the high-density matter models. We explore the possible parametrization models based on constraints from terrestrial experiments and astrophysical observations (viz. massive NSs, radii estimations of NSs, gravitational-waves emitted during the inspiral phase of binary neutron star coalescence) on dense matter EoS. To construct the EoS, we consider non-linear Walecka (NLW) type and density-dependent (DD) meson-baryon couplings within RMF model with exotic degrees of freedom in addition to nucleons. The phenomenological EoS models based on mean-field approximation theories and realistic nuclear potentials have been analysed considering matter composition to be only nucleonic [Malik et al., 2018; Nandi et al., 2019; Kanakis-Pegios and Moustakidis, 2020]. Therefore, this chapter will explore the novel aspects of RMF model parametrizations that satisfy the recent astrophysical observable estimations considering hyperonization, onset of meson condensations and Δ-baryons to be a viable energetic argument.

This chapter is based on the work Thapa et al. [2021] and is organized as follows. Sec.-5.2 mentions the RMF model formalism (NLW and DD) (extension to heavier baryons in β-equilibrated nuclear matter which was previously described in chapter-4). The coupling parameters incorporated in this work are described in sec.-5.3. Sec.-5.4 provides the results and finally the conclusions are summarized in sec.-5.5.

5.2 Formalism

The theoretical framework of DD coupling scenario to construct the dense matter EoS for baryon octet as well as Δ-resonances is already described in sec.-4.2. The interaction between non-strange baryons are described via the exchange of isoscalar-scalar σ, isoscalar-vector ω, and isovector-vector ρ mesons. For the hyperonic sector interactions, an additional hidden strangeness isoscalar-vector ϕ meson is taken into consideration. The role of σ^*-meson in the hyperon-hyperon interaction is not yet ascertained from past studies. It was reported to be weak in Ref.-Schaffner and Mishustin [1996]; Char and Banik [2014]. Furthermore, inclusion of the scalar hidden strangeness meson softens the EoS. Thus, to avoid ambiguity we have not considered the contribution from σ^*-meson in this particular study. For the NLW coupling model, the total Lagrangian density describing the baryon-meson interactions is given by [Glendenning and Schaffner-Bielich, 1999]

$$\begin{aligned}\mathcal{L} = &\sum_{b\equiv N,Y} \bar{\psi}_b(i\gamma_\mu D^\mu_{(b)} - m^*_b)\psi_b + \sum_l \bar{\psi}_l(i\gamma_\mu\partial^\mu - m_l)\psi_l + \sum_\Delta \bar{\psi}_{\Delta\nu}(i\gamma_\mu D^\mu_{(\Delta)} - m^*_\Delta)\psi^\nu_\Delta \\ &+ \frac{1}{2}(\partial_\mu\sigma\partial^\mu\sigma - m^2_\sigma\sigma^2) - \frac{1}{4}\omega_{\mu\nu}\omega^{\mu\nu} + \frac{1}{2}m^2_\omega\omega_\mu\omega^\mu - \frac{1}{4}\boldsymbol{\rho}_{\mu\nu}\cdot\boldsymbol{\rho}^{\mu\nu} + \frac{1}{2}m^2_\rho\boldsymbol{\rho}_\mu\cdot\boldsymbol{\rho}^\mu \\ &- \frac{1}{4}\phi_{\mu\nu}\phi^{\mu\nu} + \frac{1}{2}m^2_\phi\phi_\mu\phi^\mu - \left(\frac{1}{3}g_2\sigma^3 + \frac{1}{4}g_3\sigma^4\right)\end{aligned} \tag{5.1}$$

where the fields ψ_b, ψ_l, ψ^ν_Δ correspond to the baryon octet, lepton (Dirac) and Δ-baryon (Rarita-Schwinger) fields. The last two scalar self-interaction terms in eqn.-(5.1), are necessary to reproduce the empirical values of incompressibility. The covariant derivative $D^\mu_{(j)}$ is defined in eqn.-(4.2) with 'j' denoting the baryons. Furthermore, the Dirac and Rarita-Schwinger effective baryon masses are given by $m^*_j = m_j - g_{\sigma j}\sigma$, where m_j denotes the bare mass. The field equations are derived from the Lagrange's equation of motion and given in eqn.-(4.4). In case of NLW model, the rearrangement term does not come in to picture, with which the energy density and matter pressure expressions are given in eqns.-(4.11) and (4.13) respectively.

5.3 Coupling parameters

In this work, we adopt the NLW and DD-RMF coupling models as mentioned in chapter-2 for meson-baryon couplings.

Comparison of experimental data [Oertel et al., 2017] from finite nuclei and heavy-ion collisions with different microscopic model calculations have provided bounds on nuclear saturation properties of symmetric nuclear matter (SNM):

1. Incompressibility, 210 MeV $\leq K_0(n_0) \leq$ 280 MeV,
2. Symmetry energy coefficient, 28.5 MeV $\leq E_{\rm sym}(n_0) \leq$ 34.9 MeV,
3. Slope parameter of $E_{\rm sym}$, 30.6 MeV $\leq L_{\rm sym}(n_0) \leq$ 86.8 MeV.

Table-2.2 displays the nuclear saturation properties obtained for models with different RMF parametrizations considered in this work. The density-dependent coupling relations and the corresponding coefficient values are provided in chapter-2.

The meson-hyperon and meson-Δ couplings are considered similar to the density-dependence footing in the case of nucleons in DD RMF model. In the case of the meson-hyperon vector couplings, we implement the SU(6) symmetry and quark counting rule [Schaffner et al., 1994]. For the scalar meson-hyperon couplings, we consider the optical potentials of Λ, Σ and Ξ-hyperons in SNM to be $-28, +30$ and -14 MeV, respectively, at nuclear saturation [Feliciello and Nagae, 2015; Gal et al., 2016].

Due to scarce information regarding the Δ-nucleon interactions, we treat the meson-Δ resonances couplings as parameters. In the ensuing discussion, we will consider $x_{\omega\Delta} = 1.10$, $x_{\rho\Delta} = 1.00$ for the vector meson-Δ baryon couplings and $x_{\sigma\Delta} = 1.20$ for the scalar coupling. For further information regarding the Δ-potentials evaluated and implemented in various models and works, the readers may refer to sec.-4.3.2.

5.4 Constraints on dense matter models

In this section, we sort out the different EoSs with various possible compositions and parametrizations based on terrestrial experimental and stellar observational values. From table-2.2 it can be noticed that all the models reproduce n_0 and E_0 in the correct range of empirical values. However, among the NLW parametrizations considered in this work, GM1 and GM2 cannot reproduce the empirical range of K_0 at n_0 mentioned in sec.-5.3, while all the DD RMF models considered in this work satisfy the empirical range of K_0 at n_0. On the other hand, the empirical range of symmetry energy coefficient is satisfied by GM1, GM2 and GM3 parameter sets among NLW models, while in the case of DD models, all except PKDD parametrization lies within the bounds of this particular saturation property. The current empirical bound on $L_{\rm sym}$ is satisfied by all DD parametrization models considered in this work except PKDD parametrization. Fig.-5.1 displays the parameter sets which are compatible with the current bounds on $E_{\rm sym}$ and $L_{\rm sym}$. All the DD models (except PKDD) considered in this work satisfy the current bounds on nuclear saturation properties.

The mass-radius (M-R) relations corresponding to the various parametrizations for only nucleonic matter composition, are shown in upper panel of fig.-5.2 obtained by solving the TOV equations for spherically symmetric, non-rotating stars. For the crustal region, the Baym, Pethick and Sutherland (BPS) [Baym et al., 1971b] and Baym, Bethe, Pethick (BBP) [Baym et al., 1971a] EoSs are implemented. The transition from crust to the core is modelled in a way that is thermodynamically consistent following Fortin et al. [2016]. We consider the recent massive NS observation (PSR J1810 + 1744) as the lower bound for maximum mass configurations. If we consider pure nucleonic matter, all the EoSs considered in this work except a few satisfy the lower bound constraint of maximum mass as evident from the upper panel of fig.-5.2. GM2 ($M_{\rm max} \sim 2.08\ M_\odot$), GM3 ($2.02\ M_\odot$) among NLW type and TW99 ($2.07\ M_\odot$), DDV ($1.93\ M_\odot$), DDF ($1.96\ M_\odot$) among DD type models fail to satisfy this mass constraint. However, the constraints obtained from NICER observations (PSR J0030 + 0451) are seen to be not satisfied by the NLW models fulfilling mass constraint, except the GM1 parametrization, while all the DD type models satisfying the mass constraint satisfy this constraint too. Moreover, these models satisfy the recent NICER results of PSR J0740 + 6620 simultaneously. Here, PSR J0740 + 6620 observation suggests the dense matter at higher densities is repulsive enough to produce large radii of heavier NSs. Most of the NLW models not satisfying the NICER observations of PSR J0030 + 0451 are observed to satisfy this recent constraint with a wider radii range. However, even though they are observed to fulfil the

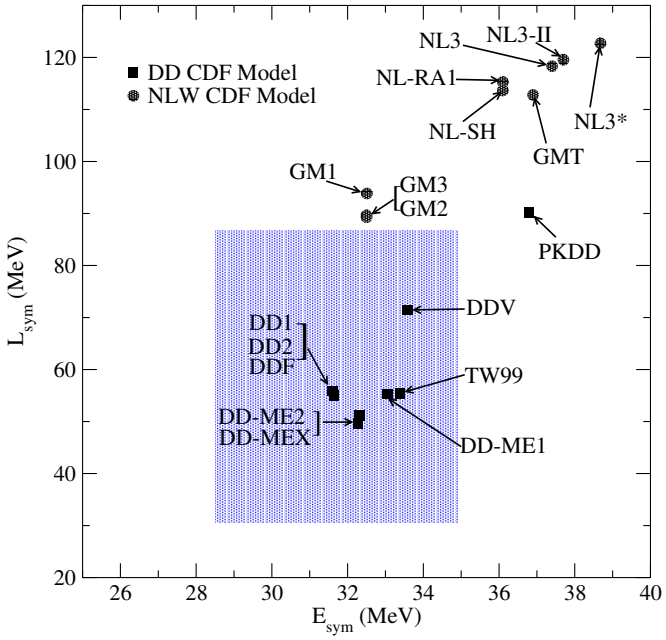

Figure 5.1: Symmetry energy coefficient ($E_{\rm sym}$) and its corresponding slope parameter ($L_{\rm sym}$) for all the parametrization models considered in this work. The shaded region represents the current empirical range in $E_{\rm sym}-L_{\rm sym}$ plane following recent experimental and microscopic model calculations [Oertel et al., 2017].

constraint from Miller et al. [2021], they fail to fulfil another NICER measurement of PSR J0030+0451 from Miller et al. [2019]; Riley et al. [2019]; Jiang et al. [2020]; Landry et al. [2020]. Stiffer EoSs (N-matter) obtained from NLW type parametrizations (except GM1, GM2, GM3) and DD-MEX (DD type) yield $M_{\rm max} \geq 2.5\ M_\odot$ satisfying the GW190814 event secondary component's mass constraint. This constraint is not unequivocal as the nature of secondary compact object is not guaranteed to be a NS [Sedrakian et al., 2020; Jie Li et al., 2020]. The TOV results involving different parametrizations with pure N-matter are summarized in table-5.1. As a result of EoS softening due to the inclusion of hyperons and Δ-quartet, the only NLW model EoS with the GM1 parametrization, satisfying all mass-radius constraints, produce stars that fail to fulfil the lower bound constraint of maximum mass as shown in the lower panel of fig.-5.2. Except PKDD ($M_{\rm max} \sim 1.93\ M_\odot$), DD1 ($\sim 2.05\ M_\odot$) and DD2 ($\sim 2.06\ M_\odot$) parametrizations all other parametrizations from DD RMF models which satisfy the joint constraints from PSR J1810 + 1744, PSR J0740 + 6620 and PSR J0030 + 0451 with pure N-matter satisfy the mass constraints even after softening due to hyperonization. The incorporation of Δ-quartet reduces the radii of NSs, enhancing their respective compactness parameter.

We now look into the pressure bounds in lower and higher density regimes derived from GW170817 event data. Fig.-5.3 shows that all the EoSs with pure nuclear matter satisfying mass-radius constraints also satisfy both the pressure bounds. It is to be noted that among NLW models, GM1, GM2 and GM3 satisfy only the lower bound at $n \sim 2n_0$ while they fail to satisfy the bound at $n \sim 6n_0$. It has to be kept in mind that the estimated bound at $6n_0$ is more than the central pressures of compact stars involved in GW170817 event.

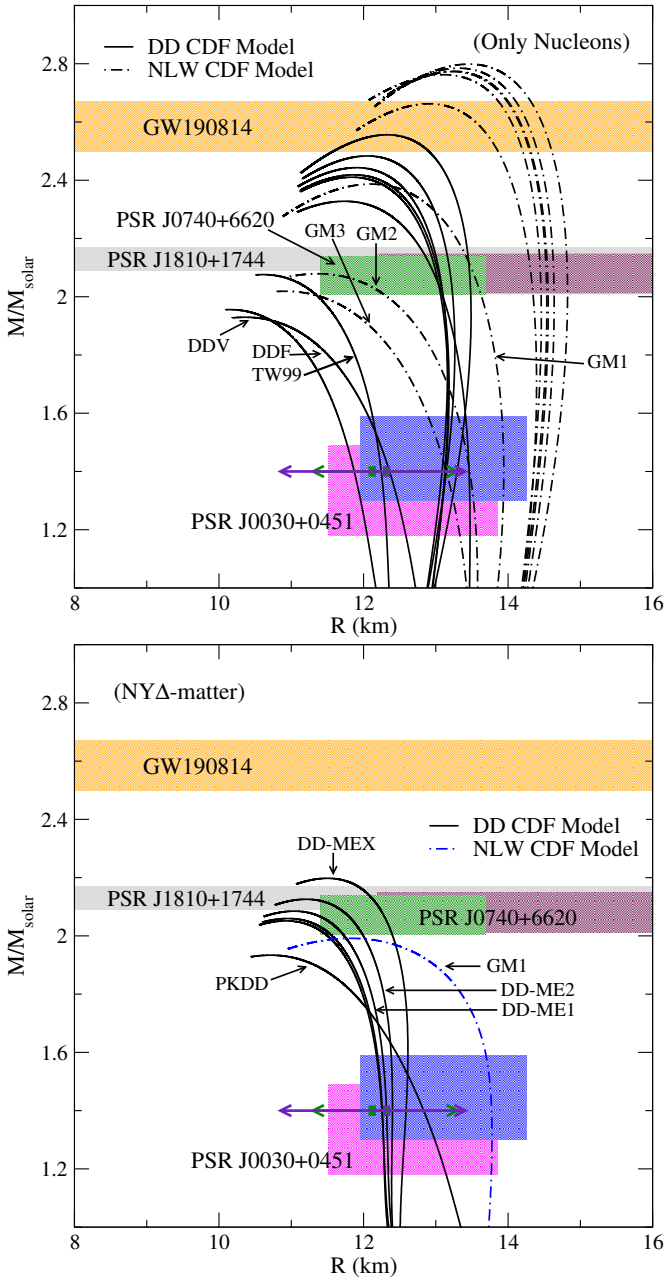

Figure 5.2: The family of solutions of TOV equations for matter composed of, upper panel: only nucleons and lower panel: Δ-admixed hypernuclear matter alongside leptons to maintain β-equilibrium. The solid curves denote the M-R curves for different density-dependent model parametrizations, while the dot-dashed curves denote the cases with non-linear scalar model parametrizations. The astrophysical constraints from GW190814 [Abbott et al., 2020b], PSR J1810 + 1744 [Romani et al., 2021], PSR J0030 + 0451 [Miller et al., 2019; Riley et al., 2019; Jiang et al., 2020; Landry et al., 2020], PSR J0740 + 6620 [Riley et al., 2021; Miller et al., 2021] are represented by the shaded regions.

We have evaluated $\tilde{\Lambda}$ with the range of primary and secondary masses $1.36 - 1.60\ M_\odot$ and $1.17 - 1.36\ M_\odot$ respectively to provide the chirp mass, $\mathcal{M} = (M_1 M_2)^{3/5}(M_T)^{-1/5} = 1.188\ M_\odot$ where the total mass $M_T = M_1 + M_2$, is in the range $2.73 - 2.78\ M_\odot$ for GW170817 event. In this work, we have considered the source properties to be circumscribing within 90%

Table 5.1: Summary of TOV results evaluated from parameter sets considered in this work (pure N-matter, refer to upper panel of fig.-5.2). Fulfillment of the mass-radius constraints from various astrophysical observations are marked by $+(-)$.

RMF Model		PSR J0030 + 0451	PSR J0740 + 6620	PSR J1810 + 1744	GW190814 (secondary)**
	GM1	+	+	+	−
	GM2	+	+	−	−
	GM3	+	−	−	−
	NL3	−	+	+	+
NLW	NL3-II	−	+	+	+
	NL-SH	−	+	+	+
	NL-RA1	−	+	+	+
	NL3*	−	+	+	+
	GMT	−	+	+	+
	DD1	+	+	+	−
	DD2	+	+	+	−
	DD-ME1	+	+	+	−
	DD-ME2	+	+	+	−
DD	PKDD	+	+	+	−
	TW99	+	−	−	−
	DDV	+	−	−	−
	DDF	+	−	−	−
	DD-MEX	+	+	+	+

** The nature of secondary component of GW190814 is still an open question

credible intervals. Fig.-5.4 shows the $\tilde{\Lambda}$ variation with mass-ratio parameter (q). $\tilde{\Lambda}$ is found to be almost independent of the mass asymmetry factor q (refer to table-5.2 for numerical results). In the left panel, curves are for pure nucleonic matter and in the right panel, they are for Δ-admixed hypernuclear matter. For pure nucleonic matter, only GM2, GM3 models lie within the observational $\tilde{\Lambda} \sim 900$ bound among the NLW RMF models. However, they do not satisfy the lower bound constraint of maximum mass. In DD RMF models, all parametrizations considered in this work follow the upper bound of 900. The stringent limit of $\tilde{\Lambda} \sim 720$ is observed to be satisfied by only TW99, DDV, DDF models which do not satisfy lower bound constraint for maximum mass. With Δ-baryons coming into the picture, the models fulfil the latter stringent upper bound on $\tilde{\Lambda}$ as shown from the right panel of the figure. Since the effect of hyperon inclusion on $\tilde{\Lambda}$ is similar to that of nucleons for the NSs with mass bounds obtained from GW170817 event, so they are not shown in fig.-5.4.

Similar to fig.-5.4, the effective tidal deformability as a function of mass-asymmetry factor q corresponding to the GW190425 event with a fixed chirp mass, $\mathcal{M} = 1.43\ M_{\odot}$ for all the parametrizations considered in this work is shown in fig.-5.5 with only nucleonic matter.

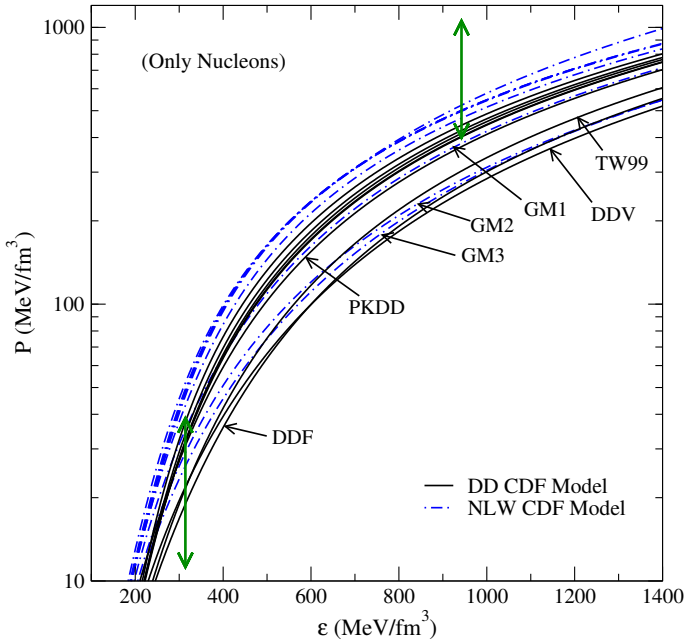

Figure 5.3: The variation of matter pressure as a function of energy density for β-equilibrated matter composed of only nucleons and leptons. The solid curves denote the EoSs for different density-dependent model parametrizations, while the dot-dashed curves denote the cases with non-linear scalar model parametrizations. The constraints on matter pressure evaluated from GW170817 event are denoted by the vertical lines and provided in sec.-5.1.

In this case, masses of the two compact stars are varied in the ranges $1.60 \leq M_1/M_\odot \leq 1.87$ (primary) and $1.46 \leq M_2/M_\odot \leq 1.69$ (secondary) [Abbott et al., 2020a]. Weak dependece of $\tilde{\Lambda}$ on q can be inferred. It is observed that all the parametrizations satisfy the upper bound constraint on $\tilde{\Lambda}$ provided by GW190425 event data. Consequently this GW event does not provide enough information to put strict limits on constraining dense matter EoSs. Inclusion of Δ-quartet will decrease $\tilde{\Lambda}$ compared to pure nucleonic case.

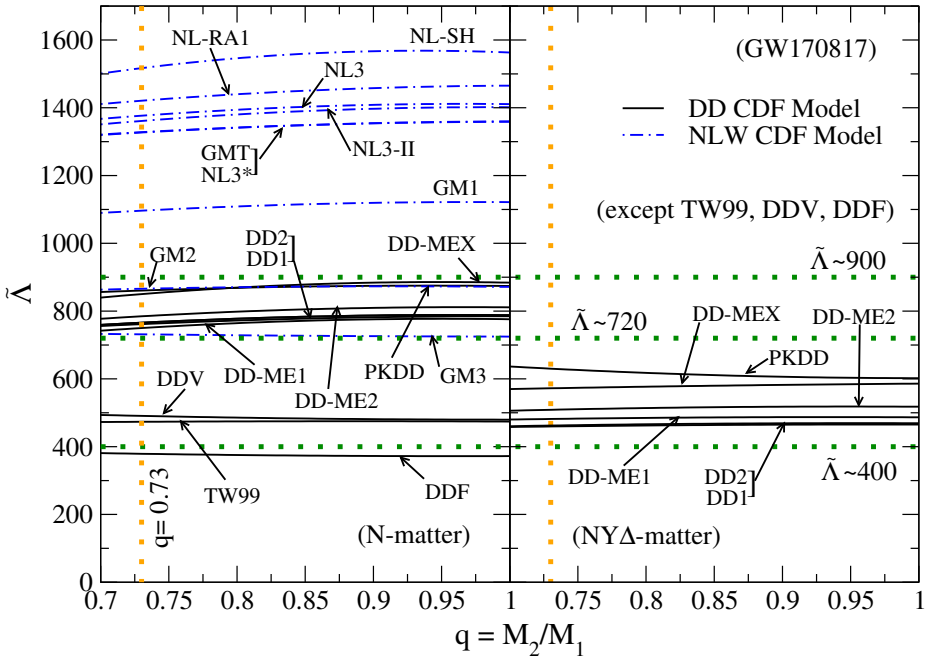

Figure 5.4: Combined dimensionless tidal deformability as a function of mass-ratio (q) considering a fixed chirp mass, $\mathcal{M} = 1.188\ M_{\odot}$ (GW170817 event). Left panel: nucleonic matter, right panel: Δ-resonances and baryon octet matter. The solid, dot-dashed lines depicts the DD and NLW type parametrizations respectively. The parametrizations yielding soft EOSs are not shown in the right panel. The horizontal dotted lines denote bounds on $\tilde{\Lambda}$ (with 90% credibility, low-spin priors). The vertical dotted lines represent the mass-ratio, $q = 0.73$ boundary [Abbott et al., 2019].

Table 5.2: Observational properties of various RMF models with different matter compositions. Here, q represents the mass ratio of the secondary component (M_2) to primary one (M_1) involved in GW event. $C_{1.4}$ denotes the compactness parameter for a $1.4M_\odot$ NS.

Matter composition	RMF Model	$M_{\max}$ ($M_\odot$)	$R_{1.4}$ (km)	$\Lambda_{1.4}$	$C_{1.4}$	$\tilde{\Lambda}$ ($q = 0.8$)		$\tilde{\Lambda}$ ($q = 1.0$)	
						GW170817	GW190425	GW170817	GW190425
Pure Nucleonic Matter	GM1	2.387	13.939	966.34	0.148	1109.39	355.77	1121.63	358.93
	GM2	2.079	13.468	743.19	0.153	870.59	246.12	871.51	244.33
	GM3	2.019	13.146	607.88	0.157	724.64	189.05	728.79	184.81
	NL3	2.774	14.430	1222.72	0.143	1394.86	489.88	1410.87	495.58
	NL3-II	2.773	14.408	1217.59	0.143	1381.14	483.69	1401.64	494.33
	NL-SH	2.799	14.630	1368.94	0.141	1547.36	554.41	1563.07	565.93
	NL-RA1	2.785	14.490	1278.05	0.143	1440.78	508.58	1465.28	518.21
	NL3*	2.762	14.355	1181.41	0.144	1341.70	465.63	1358.48	476.51
	GMT	2.662	14.355	1177.91	0.144	1342.24	456.92	1359.93	462.36
	DD1	2.410	13.126	678.92	0.157	772.75	259.42	784.91	261.88
	DD2	2.418	13.133	683.97	0.157	778.13	261.79	787.99	265.77
	DD-ME1	2.443	13.086	672.37	0.158	765.14	261.09	776.04	266.31
	DD-ME2	2.483	13.146	706.08	0.157	798.93	276.48	811.16	281.47
	PKDD	2.328	13.461	750.66	0.154	869.05	273.56	874.03	275.28
	TW99	2.076	12.245	402.46	0.169	474.17	134.40	474.57	133.73
	DDV	1.929	12.360	398.67	0.167	485.52	117.40	479.76	112.95
	DDF	1.956	11.871	311.618	0.174	372.22	94.59	375.27	91.84
	DD-MEX	2.556	13.293	773.49	0.156	869.28	309.58	883.91	316.32
Hypernuclear Matter	DD1	2.039	13.124	680.44	0.158	777.19	262.33	783.48	264.47
	DD2	2.046	13.132	684.61	0.157	784.18	265.08	793.09	267.20
	DD-ME1	2.075	13.086	673.16	0.158	773.05	265.19	778.05	267.71
	DD-ME2	2.115	13.146	707.53	0.157	808.16	277.39	813.83	282.33
	PKDD	1.943	13.444	744.97	0.154	866.23	269.07	870.23	273.08
	DD-MEX	2.186	13.293	773.49	0.156	873.62	312.38	884.72	319.36
Δ-admixed Hypernuclear Matter	DD1	2.052	12.254	398.11	0.169	462.63	137.06	465.33	138.56
	DD2	2.059	12.260	402.03	0.169	466.22	139.86	469.16	140.69
	DD-ME1	2.085	12.320	418.19	0.168	485.03	146.52	486.65	148.15
	DD-ME2	2.126	12.400	444.20	0.167	514.21	160.55	517.89	163.58
	PKDD	1.934	12.832	501.68	0.161	617.18	144.53	602.05	136.74
	DD-MEX	2.198	12.588	503.30	0.164	577.19	189.24	586.07	192.52

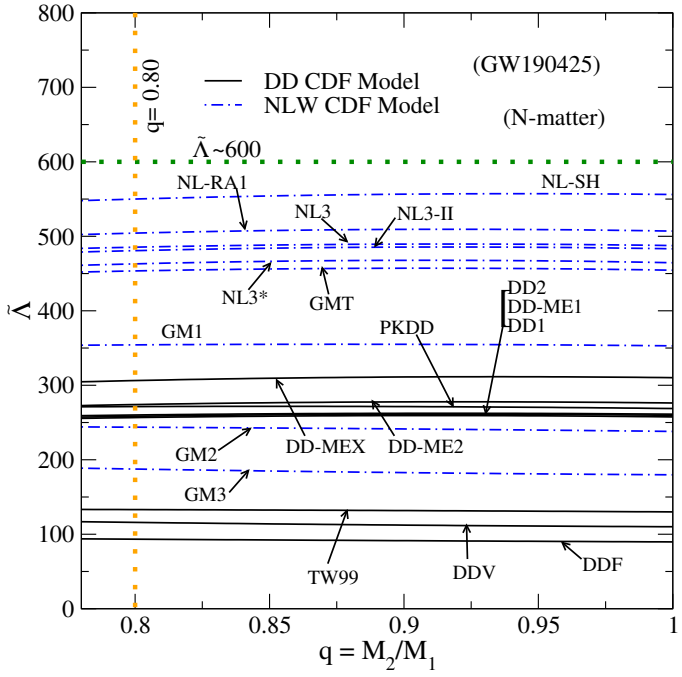

Figure 5.5: Similar to fig.-5.4 but considering a fixed chirp mass, $\mathcal{M} = 1.43\ M_\odot$ (GW190425 event) with pure nucleonic matter. The solid, dot-dashed lines depicts the DD and NLW type parametrizations respectively. $\tilde{\Lambda}$ constraints are similar to fig.-5.4. The vertical dotted lines represent the mass-ratio, $q = 0.80$ boundary [Abbott et al., 2020a].

We next evaluate the tidal deformabilities (Λ_1, Λ_2) of binary components involved in GW170817 event with different matter compositions. For the evaluation of Λ_1 and Λ_2, we consider $\mathcal{M} = 1.188\ M_\odot$ where $M_T = 2.73 - 2.78\ M_\odot$. The masses of the two components are varied in $1.36 \leq M_1/M_\odot \leq 1.60$ (primary) and $1.17 \leq M_2/M_\odot \leq 1.36$ (secondary) ranges [Abbott et al., 2017c]. From the left panel of fig.-5.6, it is observed that for pure nucleonic matter the NLW RMF model parametrization GM1 do not lie within the 90% probability contours of $\tilde{\Lambda} \sim 900$, although GM2 and GM3 do, while in case of DD RMF models, all the parametrizations lie inside these $\tilde{\Lambda} \sim 900$ contours. In the case of matter composition as NY, the tidal deformability is quite similar to the ones with pure nucleonic matter and hence not shown in fig.-5.6. In case of Δ-resonance admixed hypernuclear matter, for all the relevant EOSs Λ_1, Λ_2 falls well even within the $\tilde{\Lambda} \sim 720$ probability contour (obtained from recent reanalysis) as shown in the right panel of the figure. Table-5.2 provides the numerical estimates of various observational properties of different RMF models considering matter composition to be purely nucleonic, hypernuclear and Δ-resonance admixed hypernuclear matter.

Next we attempt to restrict radius of compact stars by evaluating $\tilde{\Lambda}$ with particular star combinations for both the events considering different parametrization models. For the event GW170817, we have taken $M_1 = 1.50\ M_\odot$ and $M_2 = 1.24\ M_\odot$ and for the event GW190425 we have taken $M_1 = 1.70\ M_\odot$ and $M_2 = 1.59\ M_\odot$ where, M_1, M_2 correspond to primary and secondary components respectively. We plot the values of $\tilde{\Lambda}$ with radius of the primary star

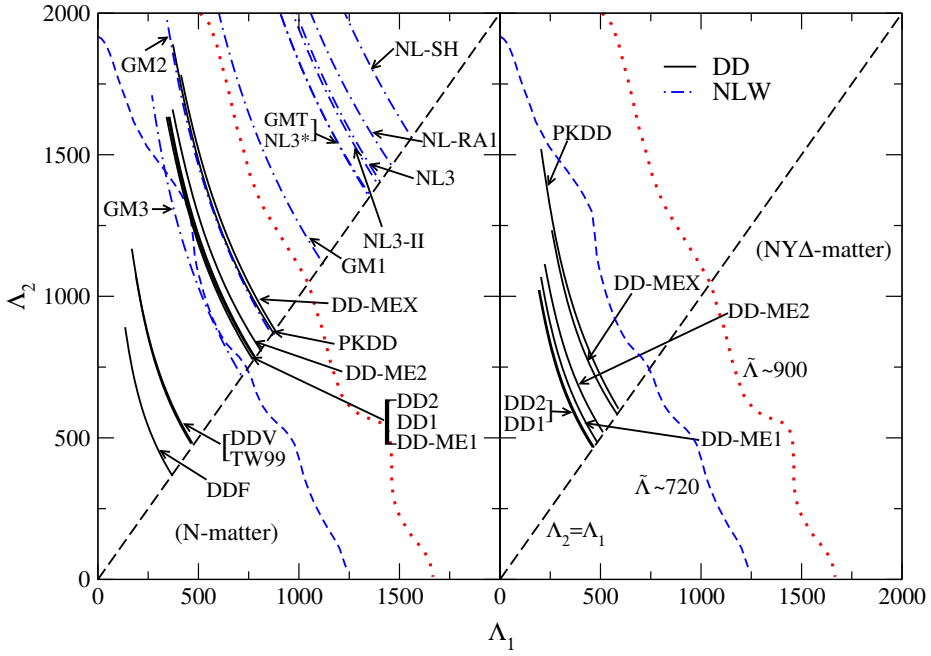

Figure 5.6: Tidal deformability parameters Λ_1, Λ_2 corresponding to the binary components, M_1, M_2 for GW170817 event with matter composition as, left panel: pure nucleonic matter, right panel: Δ-baryon admixed hypernuclear and assuming a fixed chirp mass, $\mathcal{M} = 1.188\ M_\odot$. The solid curves denote the DD type parametrizations while the NLW type are denoted by dash-dotted curves. The dotted, short-dashed curves denote the $\tilde{\Lambda} \sim 900$ (TaylorF2), 720 (PhenomPNRT) upper bounds at 90% confidence level (low-spin priors) respectively [Abbott et al., 2017c, 2019]. The diagonal long-dashed line marks $\Lambda_1 = \Lambda_2$ case.

for respective EoSs in fig.-5.7. Tight correlations between $\tilde{\Lambda}$ and $R(M_1)$ are given by the fits

$$\tilde{\Lambda}^{(\mathrm{GW170817})}_{\mathrm{fit}} = 7571 - 1423R(M_1) + 68.93(R(M_1))^2,$$
$$\tilde{\Lambda}^{(\mathrm{GW190425})}_{\mathrm{fit}} = 2638 - 501.2R(M_1) + 24.34(R(M_1))^2,$$

with maximum deviations, $(|\tilde{\Lambda}_{\mathrm{fit}} - \tilde{\Lambda}|/\tilde{\Lambda}) \sim 2.65\%,\ 7.45\%$, $\chi^2 = \sum_i^{\mathcal{N}} \left[(\tilde{\Lambda}^i_{\mathrm{fit}} - \tilde{\Lambda}^i)^2/\tilde{\Lambda}^i\right] = 4.16,\ 7.16$ with $\mathcal{N} = 30$ EoS models and coefficients of determination, $\mathcal{R}^2 = 1 - SS_{\mathrm{res}}/SS_{\mathrm{total}} \sim 0.999,\ 0.996$ for GW170817, GW190425 event respectively. Here, $SS_{\mathrm{res}} = \sum_i (\tilde{\Lambda}_i - \tilde{\Lambda}^{\mathrm{fit}}_i)^2$, $SS_{\mathrm{total}} = \sum_i (\tilde{\Lambda}_i - \bar{\tilde{\Lambda}}_i)^2$ are sum of squares of the residual errors and squared error of the mean line respectively. The point where the curves cross $\tilde{\Lambda}$ bounds corresponds to limits on primary component's radius and hence the EoSs. The figure shows that the upper bound on $\tilde{\Lambda} \sim 900$ results in radius ≤ 13.44 km, which excludes certain NLW models except for GM2 and GM3 EoSs. On the other hand, if we consider the upper bound on $\tilde{\Lambda} \sim 720$, the radius bound ≤ 12.98 km not only excludes all the NLW EoSs but also matter without Δ resonances with DD parametrizations. From the lower bound of $\tilde{\Lambda} \sim 400$, the lower bound on radius ≥ 11.89 km which excludes dense matter composed of only nucleons with DDF (DD type) parametrization.

From the observation of GW190425, the upper bound on $\tilde{\Lambda} \sim 600$ provides the upper bound on the primary component's radius ≤ 15.00 km, which gives no limit on the EoSs. Similar to fig.-5.7, effective tidal deformability as a function of secondary component's radius in GW170817 and GW190425 events is shown in fig.-5.8. The correlation fits between $\tilde{\Lambda}$ and

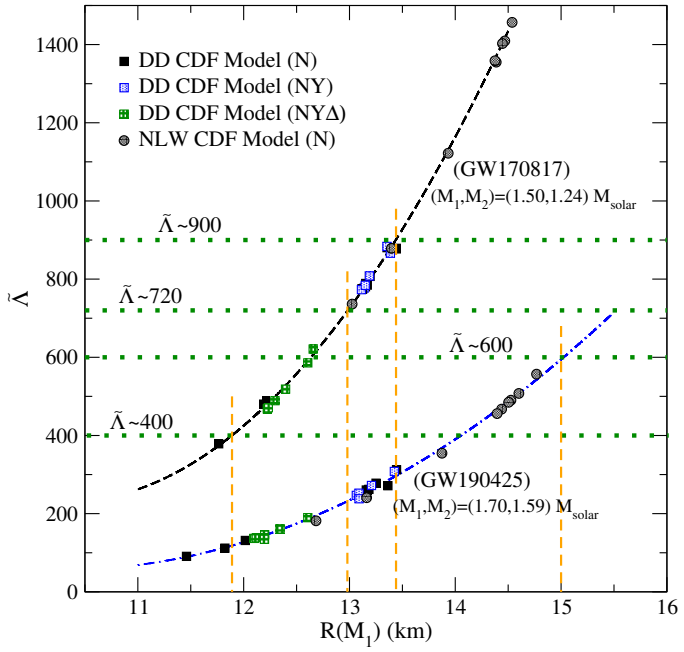

Figure 5.7: Effective tidal deformability variation with radius of the binary's primary component for GW170817 and GW190425 events. The solid, dotted, stripped squares represent the DD parametrizations with pure nucleonic, baryon octet, Δ-admixed hypernuclear matter respectively. The solid circles denote the NLW parametrizations with nucleonic matter case. The quadratic correlations for the GW170817, GW190425 cases are given by short-dashed and dash-dotted curves respectively. The horizontal dotted lines represent bounds on $\tilde{\Lambda}$ similar to figs.-5.4,5.5. The vertical short-dashed lines mark the points where the quadratic fits intersect $\tilde{\Lambda}$ bounds.

$R(M_2)$ are given by

$$\tilde{\Lambda}_{\rm fit}^{(\rm GW170817)} = 6249 - 1251R(M_2) + 63.62(R(M_2))^2,$$
$$\tilde{\Lambda}_{\rm fit}^{(\rm GW190425)} = 2783 - 527.5R(M_2) + 25.48(R(M_2))^2,$$

with maximum deviations of $\sim 17.76\%,\ 19.49\%$, $\chi^2 = 54.49,\ 17.44$ and $\mathcal{R}^2 \sim 0.983,\ 0.988$ for GW170817 and GW190425 events respectively. The upper bounds on radius for the secondary components in GW170817 case are estimated to be 13.37 km ($\tilde{\Lambda} \sim 900$) and 12.94 km ($\tilde{\Lambda} \sim 720$) while the lower bound is evaluated to be 11.99 km ($\tilde{\Lambda} \sim 400$). In case of GW190425 case, radius of the secondary component, $R_{1.59} \leq 14.99$ km ($\tilde{\Lambda} \sim 600$). From both the correlations it can be inferred that the radius bounds on NSs involved in GW events are approximately $12 \leq R_*/\text{km} \leq 13$ and $R_* \leq 15$ km in GW170817 and GW190425 events respectively.

Fig.-5.9 depicts the dimensionless tidal deformability parameter as a function of NS mass evaluated from the DD and NLW type models with matter composition to be nucleonic and Δ-commixed baryon octet. It is observed that among the NLW RMF models, GM2 and GM3 parametrizations fulfil the $\Lambda_{1.4} = 800$ upper bound (with N-matter), while they fail to satisfy the recent $\Lambda_{1.4} = 580$ bound. Other NLW parametrizations produce larger radii NSs and, as a result, are more inclined to be easily deformable since $\lambda \sim R^5$ (i.e. higher tidal deformability values). Hence no NLW model considered in this work satisfy the mass and tidal deformability constraints simultaneously. In the case of DD RMF models (with N-matter),

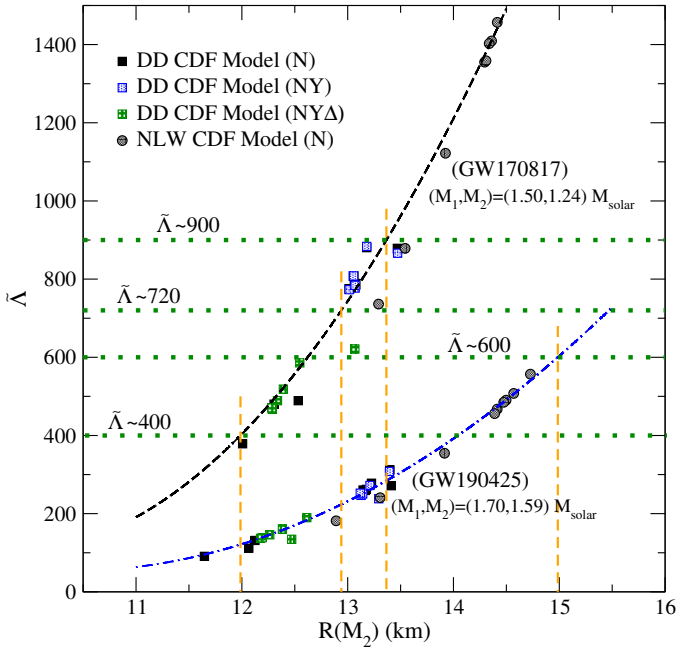

Figure 5.8: Similar to fig.-5.7 but for secondary components of GW170817 and GW190425 events. The solid, dotted, stripped squares represent the DD parametrizations with pure nucleonic, baryon octet, Δ-admixed hypernuclear matter respectively. The solid circles denote the NLW parametrizations with nucleonic matter case. The quadratic correlations for the GW170817, GW190425 cases are given by short-dashed and dash-dotted curves respectively. $\tilde{\Lambda}$ constraints are similar to fig.-5.7.

Table 5.3: Threshold densities denoted by n_u^Y (in units of n_0) for onset of hyperons in hypernuclear dense matter for various DD RMF models. $n_{1.4}^{c(Y)}$ represents the central number density for a $1.4M_\odot$ NS with hypernuclear matter composition. $\Lambda_{1.4}^N$, $\Lambda_{1.4}^{NY}$ are the dimensionless tidal deformability of a $1.4M_\odot$ NS with nucleonic and hypernuclear matter respectively.

RMF Model	$n_{1.4}^{c(Y)}$ (n_0)	n_u^Y (n_0)	$\Lambda_{1.4}^N/\Lambda_{1.4}^{NY}$
DD1	2.42	2.26	0.998
DD2	2.40	2.25	0.999
DD-ME1	2.33	2.23	0.999
DD-ME2	2.25	2.21	0.998
PKDD	2.48	2.15	1.01
DD-MEX	2.13	2.15	1.00

all the models satisfy the upper bound constraint on $\Lambda_{1.4} = 800$. However, except TW99, DDV and DDF parametrizations none of them fulfil the upper bound ($\Lambda_{1.4} = 580$) obtained from reanalysis of GW170817 event data. No coupling parameter set considered in this work is seen to satisfy the more strict constraints of $\Lambda_{1.4} = 580$ and maximum mass simultaneously with pure nucleonic matter. Another joint constraint from NICER (PSR J0030 + 0451) and GW170817 data sets an upper bound on $\Lambda_{1.4} = 730$. Recent constraint on $\Lambda_{1.4}$ obtained from Bayesian analysis provides an upper bound of 686. DD RMF models (DD1, DD2, DD-ME1, DD-ME2) are observed to satisfy these criteria inclusive with the lower bound on $M_{\rm max}$ (see

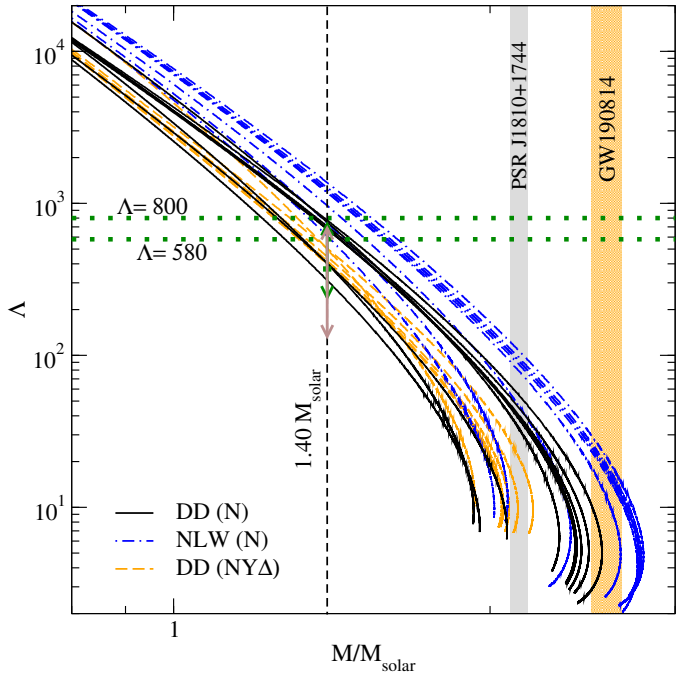

Figure 5.9: Dimensionless tidal deformability (Λ) as a function of the NS mass (M) for RMF model parametrizations considered in this work (with N, $NY\Delta$-matter). DD, NLW type models with N-matter are represented similar to fig.-5.2,5.3. While DD models with $NY\Delta$-matter are represented by long-dashed curves. The horizontal dotted lines denote the upper bounds on $\Lambda_{1.4} = 800, 580$ obtained from Abbott et al. [2017c] and recent reanalysis Abbott et al. [2019] respectively (GW170817 event). The vertical range denotes joint constraints from NICER observations (PSR J0030 + 0451) & GW170817 event [Jiang et al., 2020] and another obtained implementing Bayesian analysis [Li et al., 2021b] for a 1.4 $M_\odot$ NS. The various astrophysical constraints are similar as in fig.-5.2.

table-5.2 for numerical results). It should be noted, as evident from table-5.3 appearance of heavier baryons are inevitable in a 1.4 $M_\odot$ star with all DD RMF parametrizations except DD-MEX.

Fig.-5.10 displays the tight correlation between weighted average $\tilde{\Lambda}$ and $\Lambda_{1.4}$ tidal deformability for GW170817 event data. In this case, we have considered $M_1 = 1.40\ M_\odot$, $M_2 = 1.33\ M_\odot$ with $\mathcal{M} = 1.1878\ M_\odot$. The tight linear correlation between $\tilde{\Lambda}$ and $\Lambda_{1.4}$ is given by

$$\tilde{\Lambda}_{\rm fit}^{\rm (GW170817)} = 16.28 + 1.138\Lambda_{1.4},$$

with maximum deviation of $\sim 3.11\%$, $\chi^2 = 2.39$ and $\mathcal{R}^2 \sim 0.999$. The upper bounds on $\Lambda_{1.4}$ are deduced to be $777,\ 619$ corresponding to $\tilde{\Lambda} \sim 900,\ 720$ respectively. While the lower bound on $\Lambda_{1.4}$ based on $\tilde{\Lambda} \sim 400$ (AT2017gfo) is estimated to be 337. The upper bound on $\tilde{\Lambda}$ favours the DD parametrizations as evident from fig.-5.10.

It is noteworthy to mention that certain properties of NSs shown universal behavior or, it can be said that they are independent of any particular EoS. In this new era of GW astronomy, the relations between the tidal response parameters are found to be following universality in nature. Godzieba et al. [2021] One of such is the dependence of Λ on compactness of the

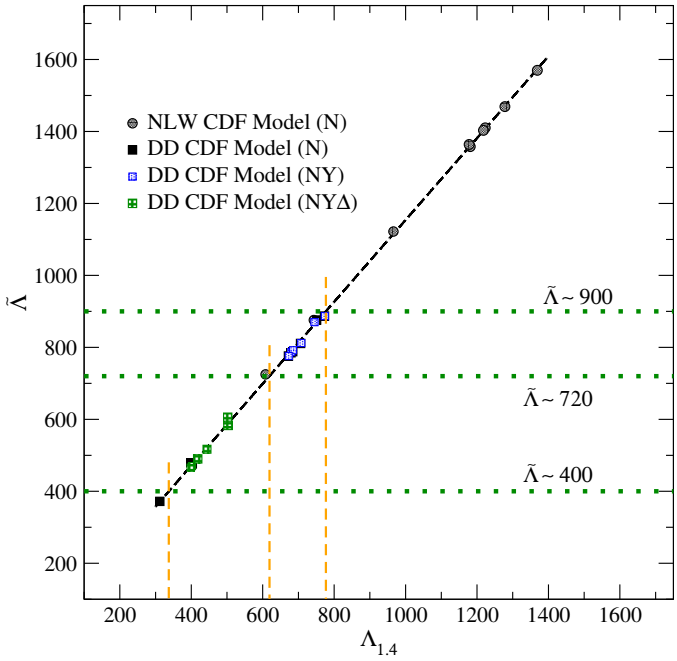

Figure 5.10: Correlation between weighted average tidal deformability and tidal deformability for 1.4 $M_\odot$ NSs. The short-dashed line denotes the best fit for the EOS data sets. The bounds on $\tilde{\Lambda} \sim 900, 720$ (upper), 400 (lower) corresponding to GW170817 event are represented by the horizontal dotted lines similar to fig.-5.7 and 5.8. The vertical short-dashed lines mark the points where the linear fit intersects $\tilde{\Lambda}$ bounds. Parametrization models involved are similar as in fig.-5.7 and 5.8.

star. Here in fig.-5.11, we have shown the same dependence for different parametrizations (with N-matter). From the figure, it is clear that the dependence of Λ on compactness is almost independent of EoSs. This relates with the result from Maselli et al. [2013]. Then in fig.-5.12, we plot the Λ for an isolated NS of mass $1.4M_\odot$ which shows a general trend with almost all EoSs. In order to find lower bound on the compactness parameter of a 1.4 $M_\odot$ NS ($C_{1.4}$), we compute the correlations between $\Lambda_{1.4}$ and $C_{1.4}$ as $\Lambda_{1.4}/10^4 = 2.094 - 22.67C_{1.4} + 62.2C_{1.4}^2$. The maximum deviation estimated is $\sim 11.94\%$ with $\chi^2 = 41.03$, $\mathcal{R}^2$ corresponding to 0.989. The stiffer NLW type parametrization models produce compact stars with larger mass and radius leading to higher tidal deformabilities. Obviously, these stiffer EOSs do not fulfil the upper limit of $\Lambda_{1.4} \leq 800$. Softer parametrizations GM2 and GM3 satisfy the upper limit of Λ. On the other hand, DD type parametrizations considered in this work generate compact stars with $\Lambda_{1.4} \leq 800$. Inclusion of Δ-resonances reduces $R_{1.4}$ resulting in increase of $C_{1.4}$ keeping Λ less than its upper limit. From fig.-5.12, it can be inferred that for a 1.4 $M_\odot$ NS, the lower bound in compactness is 0.153(0.154) corresponding to $\Lambda_{1.4} \sim 800(777)$ and it is 0.160(0.159) following the stringent upper bound of $\Lambda_{1.4} \sim 580(619)$. It also shows that the upper bound in compactness for a 1.4 $M_\odot$ NS is 0.173 following the lower bound $\Lambda_{1.4} \sim 337$. The points which lie away from the correlation fit are from GM2, GM3, PKDD coupling models. Based on the derived bounds of $C_{1.4}$, the range of $R_{1.4}$ is found to be $11.95 - 13.00$ km ($C_{1.4} \sim 0.159 - 0.173$) and $11.95 - 13.42$ km ($0.154 - 0.173$). The estimated bounds on $R_{1.4}$ satisfy the range $11.5 \leq R_{1.4}/\text{km} \leq 13.6$ as reported in Li and Steiner [2006] with the latter constrained from terrestrial experimental data.

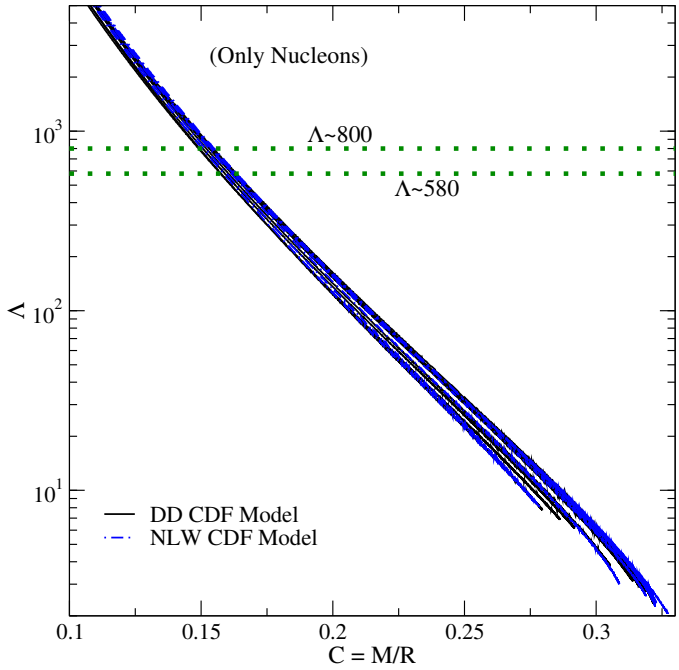

Figure 5.11: Dimensionless tidal deformability as a function of compactness parameter (C) for an isolated NS (with N-matter) for the RMF parametrizations implemented in this work. The bounds on $\Lambda \sim 800, 580$ corresponding to GW170817 event are represented by the horizontal dotted lines similar to fig.-5.9.

In addition to heavier baryons, meson such as (anti)kaon condensations may also come into the picture with rising energy density towards the interior of NSs. Thapa and Sinha [2020]; Thapa et al. [2021] reported that these meson condensations affect the lowering of maximum mass NS configurations and do not have any significant reduction in radii of $\sim 1.4\ M_{\odot}$ NSs compared to pure hadronic matter cases.

5.5 Summary

The BNS mergers provide intriguing information to constrain various theoretical formulations of dense nuclear matter EoSs. In this work, we have analysed two schemes of coupling parametrizations and tried to constrain purely nucleonic, hypernuclear, and Δ-baryon admixed hypernuclear matter EoSs within the RMF framework model via employing GW and other astrophysical observations.

Confronting the coupling parametrizations considered in this work with the recent bounds on nuclear saturation properties infers that all NLW parameter sets fail to satisfy these empirical ranges while DD coupling models (except PKDD) are seen to fulfil these bounds. In addition, imposing the lower limit of maximum mass constraint rules out the relatively softer EoSs viz. GM2, GM3 among NLW models and DDF, DDV, TW99 among DD RMF models. On the other hand, very stiff NLW EOSs, except GM1 fail to satisfy the measured radius range from observation of PSR J0030 + 0451. In the core of NSs, with higher matter density, the appearance of heavier baryons is inevitable. Their appearance softens matter,

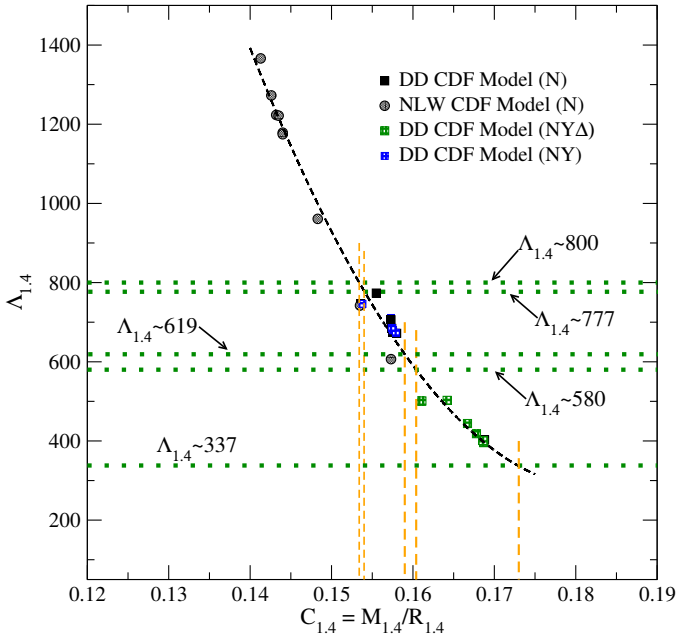

Figure 5.12: Correlation between tidal deformability and compactness parameter for 1.4 $M_\odot$ NSs. The short-dashed line denotes the best fit for the EOS data sets. The bounds on $\Lambda_{1.4}$ corresponding to GW170817 event are represented by the horizontal dotted lines similar to figs.-5.9,5.11 in addition to ones deduced from fig.-5.10. The vertical short-dashed lines mark the points where the quadratic fit intersects $\Lambda_{1.4}$ bounds. Parametrization models involved are similar as in figs.-5.7, 5.8, 5.10.

excluding additional parametrizations viz. DD1, DD2, PKDD among DD RMF models and leaving one admissible NLW model parametrization GM1. Even with pure nucleonic matter, the parametrization GM1 is ruled out because it is not soft enough to provide $\tilde{\Lambda} \leq 900$ from the GW170817 event. Hence, none of the parameter sets within NLW model considered in this work can satisfy all the observational constraints simultaneously. The upper bound on $\tilde{\Lambda} \leq 900$ allow all the parametrizations of DD RMF models, although the more strict upper limit $\tilde{\Lambda} \leq 720$ does not allow any parametrization with pure nuclear matter maintaining lower bound constraints of maximum mass. However, the appearance of heavier non-strange baryons allows all the DD RMF parametrizations to lie within the stringent upper limit.

The advent of heavier baryons (hyperons) leads to softening of EoSs, which in turn reduce the NS maximum masses values by $\sim 0.38\ M_\odot$ than that of pure nucleonic cases. The effect on dimensionless tidal deformability ($\Lambda_{1.4}$) due to the incorporation of hyperons is very marginal. It can be seen that the central number densities of $1.4M_\odot$ NSs are quite close to the onset of hyperons. This results in marginal changes in $\Lambda_{1.4}$. However, the appearance of Δ-resonances in dense matter is worthy of mentioning. From fig.-5.9, it can be seen that the value of $\Lambda_{1.4}$ lies above the stringent 580 upper bound for the stiffer DD RMF EoSs for pure nucleonic matter. With the advent of Δ-quartet, $\Lambda_{1.4}$ reduces sufficiently and moves below 580 for all stiff DD RMF parametrizations considered in this work. This relates with the results first noticed in Schürhoff et al. [2010] and subsequently discussed in Li and Sedrakian [2019] and Raduta [2021]. Δ-baryon admixed hypernuclear NSs are observed to have smaller radius values in comparison to the NSs with only baryon octet particle spectrum (refer to table-5.2).

This is due to the early onset of Δ^- baryon, which relatively softens the EoSs at lower densities.

Abbott et al. [2021] recently reported the observation of GWs from two NS-BH coalescences (GW200105 and GW200115). The masses of the NSs involved are deduced to be $1.9^{+0.3}_{-0.2}$ $M_\odot$, $1.5^{+0.7}_{-0.3}$ $M_\odot$ for the GW200105 and GW200115 events respectively. However, no constraints on tidal deformation of the secondary components have been reported. The coupling parametrizations considered in this work satisfy the NS mass constraints set by these recent GW events.

Based on the coupling data sets contemplated in this work and observed strict restrictions on $\tilde{\Lambda}$, a radius range of the NSs involved in GW170817 event is deduced to be around $12 \leq R_*/\text{km} \leq 13$ and that with GW190425 event's data is found to be $R_* \leq 15.00$ km. The lower bound on $\tilde{\Lambda}$ considered in this work is evaluated from the electromagnetic counterpart (kilonova) signal in GW170817 event. The strong correlation between weighted average $\tilde{\Lambda}$ and $\Lambda_{1.4}$ sets bounds as $337 \leq \Lambda_{1.4} \leq 619$ corresponding to $400 \leq \tilde{\Lambda} \leq 720$ in this work. Furthermore, similar analysis with strict bounds on $\Lambda_{1.4}$ translate to compactness parameter value of a 1.4 $M_\odot$ NS to be in the range $0.159 \leq C_{1.4} \leq 0.173$. This yields $R_{1.4}$ in the range $11.95 - 13.00$ km.